Cell Reports
Physical Science

CellPress
OPEN ACCESS

Article

Precisely modulated electrostatic attraction to the recognition site for on-site ultrafast visualization of trace hydrazine

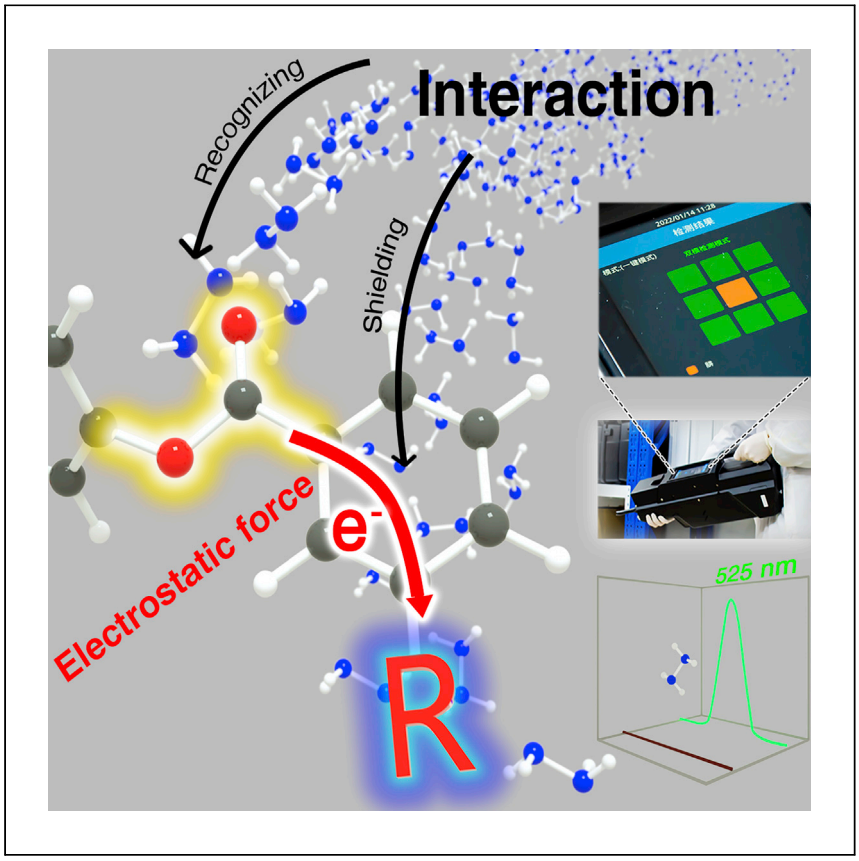

Li et al. demonstrate that the interaction between ester bond and hydrazine can be precisely modulated by the electron-withdrawing ability of the adjacent R-benzene group. The strong electrostatic attraction and moderate shielding effect of the F-CN probe promote its combination with the analyte and improve the light-up time to 2–3 s.

Jiguang Li, Zhiwei Ma, Da Lei, Baiyi Zu, Xincun Dou

xcdou@ms.xjb.ac.cn

Highlights

The combination of recognition site with analyte greatly affects the response speed

Combination efficiency relies on electrostatic attraction and shielding effect

Proposed F-CN probe enables a LOD of 2 nM and light-up time of 2–3 s for hydrazine

Exploration of a portable detector demonstrates the applicability of the F-CN probe

Li et al., Cell Reports Physical Science 3, 100878
May 18, 2022
https://doi.org/10.1016/j.xcrp.2022.100878

Cell Reports
Physical Science

CellPress
OPEN ACCESS

Article

Precisely modulated electrostatic attraction to the recognition site for on-site ultrafast visualization of trace hydrazine

Jiguang Li,[1,2,3] Zhiwei Ma,[1,2,3] Da Lei,[1,3] Baiyi Zu,[1] and Xincun Dou[1,2,4,*]

SUMMARY

The modulation of the recognition site has great potential for the development of high-performance fluorescent sensors, but the regulation of preferential combination between the recognition site and the target molecules has rarely been studied. Here, to boost the response speed of the fluorescent probe, the recognition site is regulated via design of the electron-withdrawing ability of the adjacent R-benzene group. The interaction between the ester bond and hydrazine (N_2H_4) is precisely modulated to promote effective combination between them in the pre-chemical approach part of the process. The strong electrostatic combination capability, the moderate shielding effect, and the favorable inverse Gibbs free energy barrier together ensure an improved light-up time of 2–3 s for the F-CN probe. The present investigation may facilitate further exploration of fluorescent probes for ultrasensitive and rapid chemical sensing, as well as additional work on interaction modulation for various applications.

INTRODUCTION

Fluorescent sensing, as a rapidly visualizable, highly specific, simply portable, and cost-effective imaging technique,[1–4] is of great significance in the fields of clinical diagnostics,[5] environmental monitoring,[6] explosives identification,[7,8] and others. In particular, the interaction process of selective bonding between host (fluorescent probe) and guest (analyte) molecules[9] can be realized by special and specific interaction forces. Various interactions affecting the matching of intermolecular geometry (size, shape) and the complementation of intermolecular electrical properties have been widely focused in molecular recognition for the investigation of complicated optical/electrical properties and the conformation of non-chemical reaction systems.[10,11] The main point focuses on the regulation of the interaction between fluorescent probe and analyte by rigidization,[12] solvent-effect[13] and geometry configuration,[14] typically involved in aggregation-induced emission-luminogen,[15] quantum dot,[16] and organic fluorescent probe.[17–20] For the chemical reaction system, in which the kinetic energy barrier plays a decisive role in determining whether the fluorescent probes could react with the analyte molecules, a far superior anti-interference performance could be achieved and has been widely used for the detection of nucleophilic active analytes such as electron-rich anions,[21] organophosphorus,[22] and amine.[23–28] Currently, most research concentrates on realizing the specific detection either through fluorescence sensing modes such as turn on, turn off, and ratiometric, or through fluorescence molecular structure modulation, especially from the aspect of the recognition site.[29–31] Based on the modulation of the recognition site, a series of fluorescent probes have been developed to improve

[1]Xinjiang Key Laboratory of Explosives Safety Science, Xinjiang Technical Institute of Physics and Chemistry, Key Laboratory of Functional Materials and Devices for Special Environments, Chinese Academy of Sciences, Urumqi 830011, China

[2]Center of Materials Science and Optoelectronics Engineering, University of Chinese Academy of Sciences, Beijing 100049, China

[3]These authors contributed equally

[4]Lead contact

*Correspondence: xcdou@ms.xjb.ac.cn

https://doi.org/10.1016/j.xcrp.2022.100878

the selectivity, sensitivity, and speed of detection. For instance, by modulating the bond angle or length of the B-O bond in the recognition site of the boronic acid functional group to form the identified sp^3-hybridized hydrated boronate structure in the fluorescent protein-based probe, the system can exhibit high sensitivity toward hydrogen peroxide even in the face of an indistinguishable interferent such as peroxynitrite.[32] By using olefin as the recognition site of thiols and aldehyde as the recognition site of SO_3^{2-}, a dual-site fluorescent probe was designed to accelerate the detection process and image the enzymatic conversion of cysteine to SO_2 in living cells, and a fast fluorescent response of <2 min was achieved.[33] Through the surface chelating reaction between the 3,3-diaminobenzidine recognition site modified on CdTe@SiO_2 and SeO_3^{2-}, the core-shell probe can detect Se concentrations in selenium-rich food with a limit of detection (LOD) as low as 6.68 nM (0.53 ppb), which is far superior to the previously reported fluorescent probes.[34] These results indicate that the modulation of the recognition site can facilitate remarkably the development of highly selective and sensitive fluorescent sensors, and inspire the promotion of response speed, which would be favorable for the various practical on-site applications.

It should be noted that the recognition site or active site that intrinsically determines the chemical reaction could be altered from the aspects of the electronic and geometric effects[35–38] through kinetic and thermodynamic forces. In particular, thermodynamic force is a crucial factor related to the preferential combination between recognition site and the target molecules and plays an important role in the pre-chemical reaction. Moreover, the influential factor of the thermodynamic force, such as the interaction between probe and analyte, could be helpful to establish the design strategy of fluorescent molecules in the chemical reaction system and the physical understanding to promote the corresponding fluorescence performance. However, this crucial thermodynamic factor has rarely been focused from the aspect of experimental investigation or from theoretical simulation, even with increasingly emerged fluorescent probe design addressing the recognition site.

Here, for the purpose of boosting the response speed of the fluorescent probe in the chemical reaction system from the perspective of promoting the combination between the recognition site and the analyte in the pre-chemical approaching process, the thermodynamic force of the recognition site was regulated considering the influence from the electrostatic effect and the shielding effect. Through quantum chemical and molecular dynamics (MD) analysis, it was found that the designed fluorescent probe enables a high electrostatic potential for the ester bond to strongly combine with the target electrostatically negative hydrazine (−35.96 kcal/mol), as well as a moderate shielding effect and a favorable inverse Gibbs free energy barrier, thus ensuring the effective combination with hydrazine to boost the response speed. Consequently, it showed a remarkably rapid response to hydrazine, with a time of 2–3 s to light up and 8 s to achieve a saturated brightness, which is far superior to the previously reported fluorescent probes, which generally need 600–3,600 s to respond. Moreover, the present probe also showed a highly sensitive detection performance, with a LOD as low as 2 nM (64 ppt), which is much better than the other reported fluorescence turn-on probes that usually lie in the range of 9.4–100 nM (ppb level).

RESULTS

Design strategies of the fluorescent probes

Hydrazine, as a typical biological toxic chemical with a risk threshold of 4.9 g/m^3 or 10 ppb,[39] has posed an enormous fatal threat to work-related personnel within an

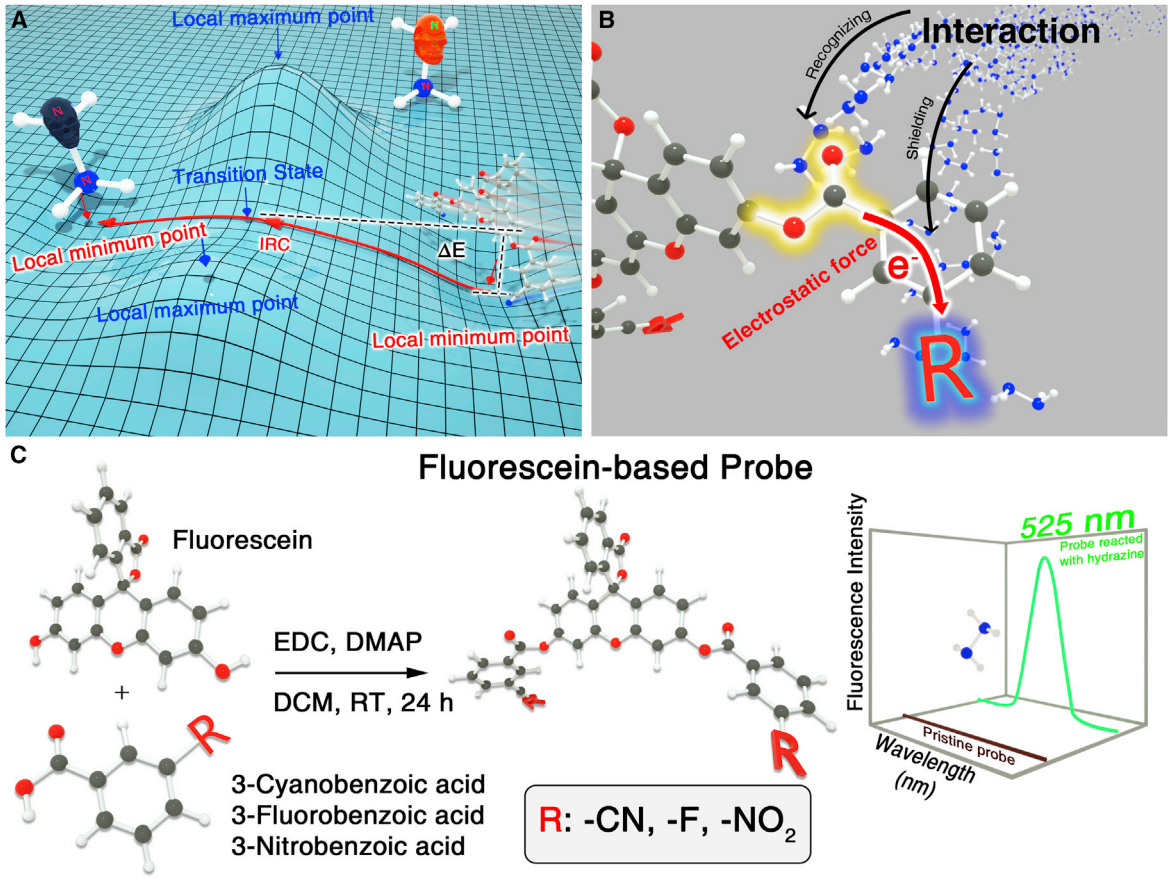

Figure 1. The modulation strategies of the recognition site on the trace hydrazine-detecting fluorescent probes

(A) The hypothetical potential energy surface of the reaction barrier decreasing method for hydrazine detection through an intrinsic reaction coordinate (IRC) path.

(B) Schematic diagram for precisely modulating the interaction between the probe and hydrazine by balancing the electrostatic force and the shielding effect that the R-benzene group brings to the recognition site.

(C) Schematic illustration of the formation of the fluorescein-based probes and their effective turn-on detection for trace hydrazine represented in fluorescent spectra.

extremely short time (several minutes) due to accidental spilling. One effective method to realize the sensitive, rapid, and reliable detection of hydrazine is to decrease the reaction barrier of the hydrazinolysis between the fluorescent probe and hydrazine (Figure 1A). Although the modulation of the reaction barrier through the design of the fluorescent probe could greatly improve the response speed, a more influential thermodynamic factor that considers the interaction between probe and hydrazine could greatly affect their combination in the pre-chemical reaction (Figure 1B). Thus, the fluorescein was esterified with 3-cyanobenzoic acid, 3-fluorobenzoic acid, and 3-nitrobenzoic acid, respectively, and three structurally similar intramolecular charge transfer (ICT) fluorescein-based probes (F-CN, F-F, and F-NO_2) were obtained through the change in R-benzene groups (R = -CN, -F, and -NO_2) to effectively modulate the combination force in the approach of hydrazine to the ester bond (Figures 1C and S1–S15; Scheme S1).

The crucial influence factors relating to the response speed

When these F-CN, F-F, and F-NO_2 ICT probes are applied in the detection of hydrazine, the ester bond of F-R acts as the recognition site and the hydrazine molecule

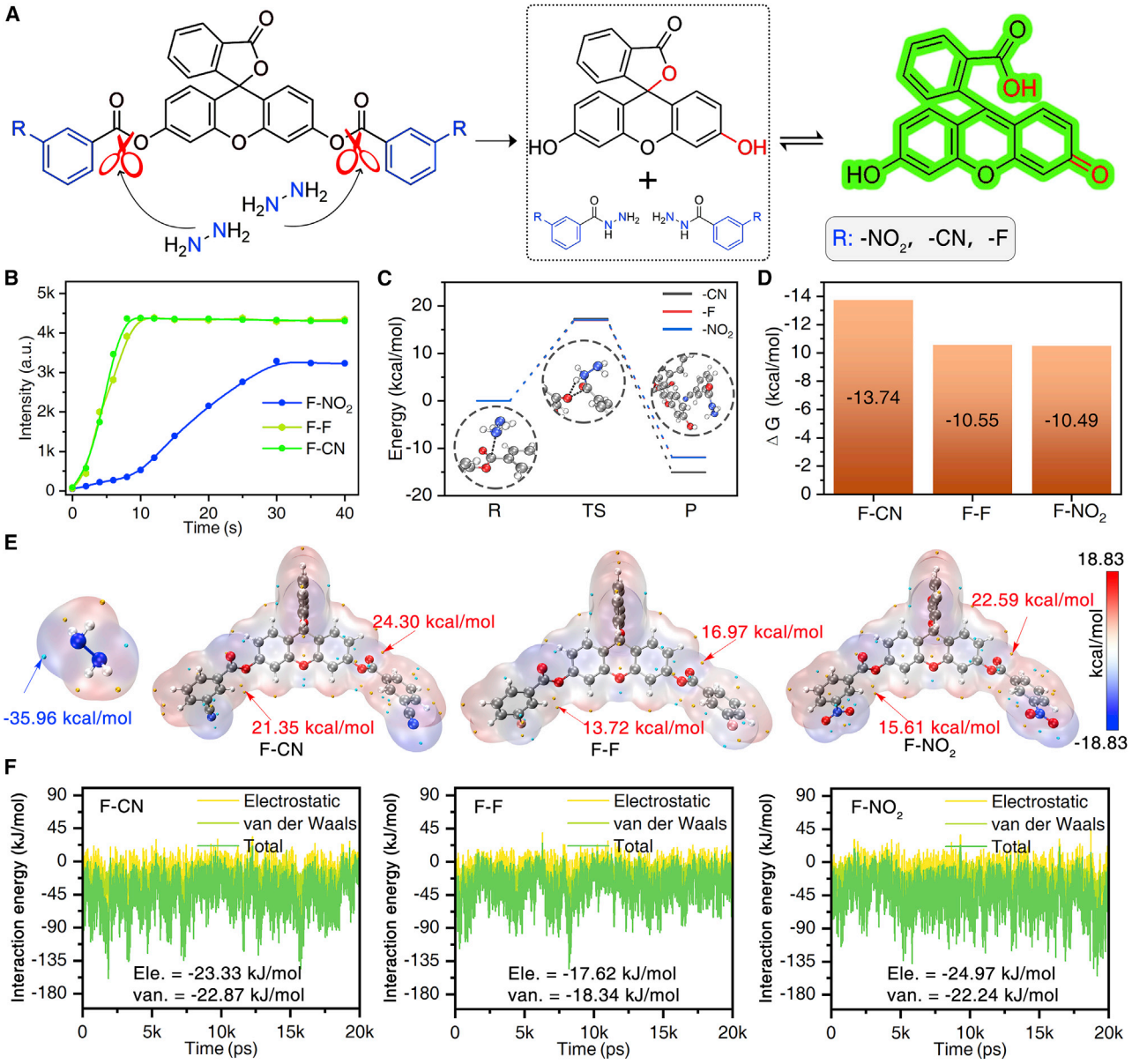

Figure 2. The thermodynamic and kinetic factors influencing the response speed of hydrazine detection

(A) Schematic illustration of the fluorescence turn-on detection of the designed probes to hydrazine.

(B) Time-dependent fluorescence response of the F-CN, F-F, and F-NO_2 probes upon the addition of the hydrazine (λ_{ex} = 365 nm; λ_{em} = 526 nm; slits: 2 nm; integral time: 100 ms; spectrometer: Maya 2000pro).

(C) Potential energy profiles for the hydrazinolysis reaction between the designed probes and the hydrazine with zero-point vibration corrected energies (kcal/mol) relative to the reactants.

(D) The Gibbs free energy difference of the reaction products for the F-CN, F-F, and F-NO_2 probes with hydrazine.

(E) The electrostatic potential distribution diagrams of the hydrazine molecule and the designed probes in which the maximal and minimum electrostatic potential surfaces presented as orange and cyan dots, respectively.

(F) The molecular dynamics simulation for the interaction energies of the 3 probes with hydrazine within a 20-ns simulation time.

attacks it to induce a bond cleavage, releasing the fluorescein of which the open-loop structure with a small ratio processes a strong green fluorescence emission and 3-R-benzohydrazide structure with no emission (Figures 2A and S16–S21). All three ICT probes can immediately display bright green fluorescence once the hydrazine solution was added into the cuvettes with different probes that can be observed

with the naked eye (Figure 2B). A further real-time detection spectrum showed that the fluorescence intensities increase from the beginning of the measurement, indicating that the three designed probes could react ultra-fast with hydrazine. To achieve the maximum fluorescence intensity, the F-CN and F-F probes need 8 and 10 s, respectively, which are much faster than that the F-NO_2 probe needs. However, besides some reported ratiometric fluorescence probes with a detection time in the range of several minutes,[40–43] the fast response of our designed probes superior to the previously reported fluorescence turn-on probes, the detection time of which usually lies in the range of 600–3,600 s (Table S1). To investigate whether the response speed difference was caused by the kinetic influential factor of the hydrazinolysis reaction, density functional theory (DFT) was applied to study the Gibbs free energy barriers (ΔE) of the reactions between these probes and hydrazine (Figure 2C). There is almost no obvious difference between all three forward ΔE, which lie in the range of 17.3–17.8 kcal/mol, indicating that these three probes could easily react with hydrazine and that their forward reaction rate constants were equally high. It is worth noting that the product resulted from the F-CN reaction system, which has the lowest energy (value of −13.74 kcal/mol), leading to the ΔE of the reverse reaction being approximately 3.2 kcal/mol higher than those of the F-F and F-NO_2 probes (values of −10.55 and −10.49 kcal/mol, respectively) (Figure 2D). This difference clearly indicates that the reverse reaction rate of the F-CN probe with hydrazine is lower than those of the other two probes, implying that the total reaction rate of the F-CN probe would be the highest and result in rapid responses of the F-CN probe. However, this kinetic analysis could not provide a reasonable explanation for the distinctly different response time between F-F and F-NO_2.

The electrostatic potential distribution diagrams show that the N atom in the hydrazine molecule has the minimum electrostatic potential, with a value of −35.96 kcal/mol due to the existence of the lone pair of electrons in the counter position of the two hydrogen atoms, indicating that hydrazine can easily attack the electron-deficient position of the probe as a nucleophile (Figure 2E). Fortunately, there are indeed two maximum electrostatic potential sites at the carbonyl carbon in the ester bond of each probe. Thus, hydrazine would be thermodynamically driven toward the carbonyl carbon and further take the nucleophilic reaction with the probe. From the perspective of the maximum electrostatic potential, the value of the carbonyl carbon site of F-CN (24.30 kcal/mol) is much higher than that of the other two probes, indicating that there is a reasonably stronger nucleophilic force between F-CN and hydrazine and leading to the fast responses of the F-CN probe. However, the value of the carbonyl carbon site of F-F (16.97 kcal/mol) is much smaller than that of F-NO_2 (22.59 kcal/mol), indicating that the F-NO_2 probe should have a faster response than the F-F probe, which still contradicts the practical result. In addition, considering the real situation influenced by the surrounding solvent molecules and the fluctuation of the system energy, the interaction within 20 ns between the probe and the hydrazine molecule in dimethyl sulfoxide (DMSO) was analyzed by MD simulation (Figures 2F and S22). It has been shown that the van der Waals energy of the F-NO_2 (−22.24 kJ/mol) probe is located between that of the F-CN (−22.87 kJ/mol) and F-F (−18.34 kJ/mol) probes, while it has the lowest electrostatic energy (−24.97 kJ/mol) compared to those of the other two probes due to the strong electron-withdrawing property of the -NO_2 group. It should be noted that the strong electrostatic interaction between F-NO_2 and hydrazine together with the favorable electrostatic potential at the carbonyl carbon in the ester bond of F-NO_2 actually would not improve the response speed. Thus, it can be concluded that the specific group largely contributes to the interaction between the probe and the analyte may weaken the effective combination between the recognition site and the analyte at the spatial level.

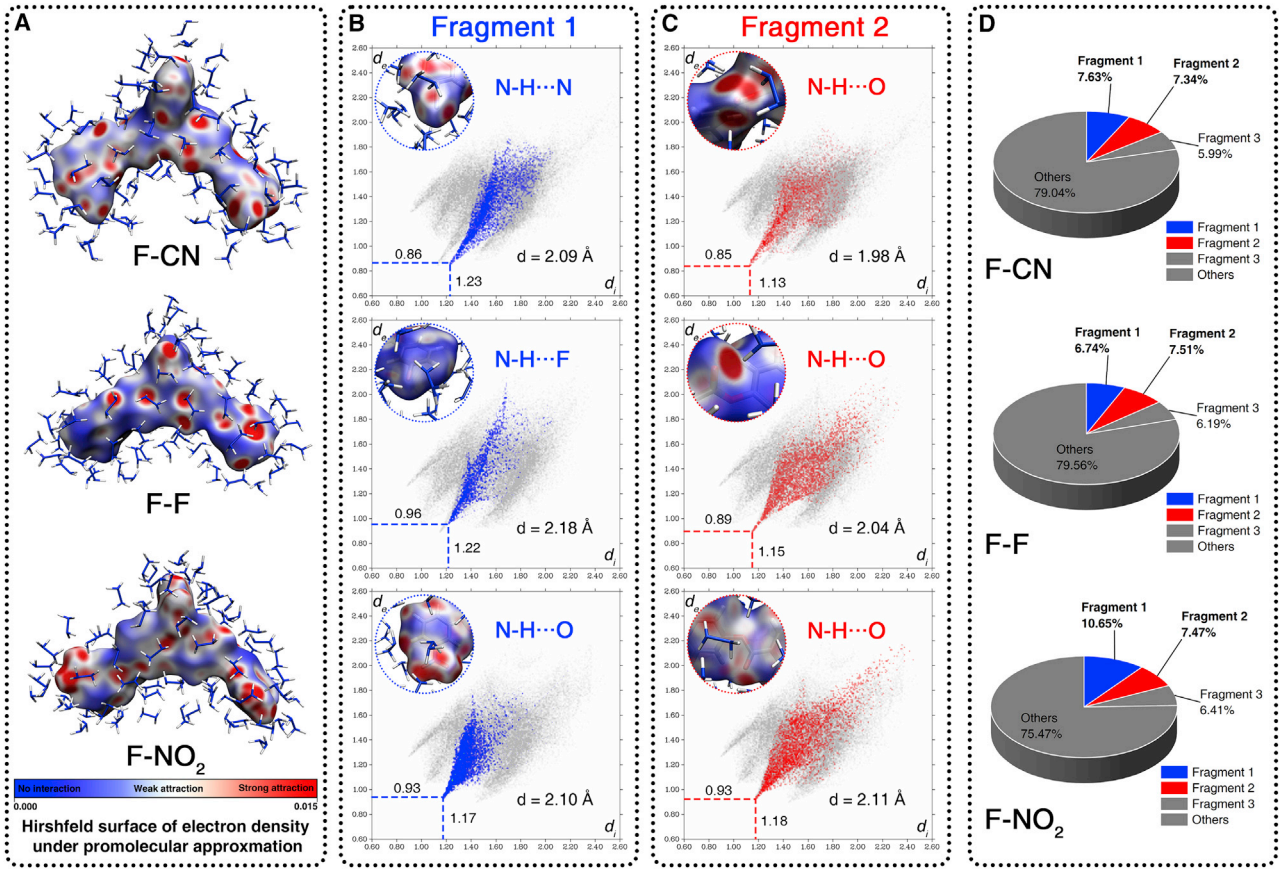

Figure 3. The Hirshfeld surface analysis of the three designed probes interacting with hydrazine

(A) The 3D Hirshfeld surfaces of the hydrazine molecules surrounding the F-CN, F-F, and F-NO_2 probes mapped by electron density under promolecular approximation cartography with a color scheme in a range of blue, white, and red, which represent no interaction, weak attraction and strong attraction, respectively.

(B and C) The 2D fingerprint plots for the local contact surface of the F-CN, F-F, and F-NO_2 probes, with the gray discrete clouds as the total Hirshfeld surface, (B) the light blue discrete clouds as fragment 1 (the R-benzene group), contributed by hydrogen bonds of N-H···N, N-H···F, and N-H···O, respectively, and (C) the light red discrete clouds as fragment 2 (the ester bond group), contributed by N-H···O.

(D) The ratios of the contact surface areas of various fragments contributed to the total Hirshfeld surface in the F-CN, F-F, and F-NO_2 probes, respectively.

To quantitatively investigate the competitive interaction of the R-benzene group with hydrazine and the ester bond with hydrazine, the Hirshfeld surface analysis was applied to qualitatively analyze the interforce at the specific area of these probes. Through various functions of distance and curvature mapped on the Hirshfeld surface, the distinct strength of the interaction between the probe and the surrounding hydrazine molecules can be demonstrated. Compared to the Hirshfeld surface of the F-F probe, which has a relatively concentrated red area located around the ester bond, both the Hirshfeld surfaces of the F-CN and F-NO_2 show a similar pattern, with the red area predominantly scattered across the surface (Figures 3A and S23). Moreover, it can be seen that the widespread red area centralizes at the -NO_2 group of the F-NO_2 probe, which is remarkably larger than the red area around the ester bond, implying that the strong electron-withdrawing -NO_2 group could pose non-negligible interference to the interaction between the recognition site and hydrazine.

From the fingerprint plots of the three probes, which were obtained by combining the distance from the internal and external nearest atom to the Hirshfeld surfaces

(defined as di and de respectively), it was found that they have many similarities reflected in the two-dimensional (2D) discrete clouds with four or five spikes (Figure 3B). To look further into the interactions between the different parts of the probe and hydrazine, the three probes were divided into three fragments corresponding to the R-benzene group, the ester bond, and the fluorescein, respectively. For the fingerprint plots of fragment 1, it was obvious that the discrete points concentrated most densely close to the top of the spike in the NO_2-benzene configuration with a total minimum value (d) of 2.10 Å, followed by the CN-benzene and F-benzene configurations, with d of 2.09 and 2.18 Å, respectively. For the fingerprint plots of fragment 2 (Figure 3C), generally there are similar sharp strips of the discrete points in the ester bond of all three probes. However, the d of the ester bond in the F-NO_2 has the highest value, 2.11 Å, which forms a sharp contrast with those in F-F (2.04 Å) and F-CN (1.98 Å), indicating that the interaction between the ester bond of the F-NO_2 and hydrazine is much weaker than those of the other two probes. Moreover, it should be noted that the d of the ester bond in the F-F probe is much lower than the d of F-benzene with 0.14 Å, while there is only a difference of 0.11 and −0.01 Å between these two values for the F-CN and the F- NO_2 probes.

Statistically, compared to the proportion that the CN-benzene and F-benzene occupy in the total Hirshfeld surface area, with values of 7.63% and 6.74% (Figure 3D), the NO_2-benzene occupies the highest proportion, with a value of 10.65%. The ester bond in the F-F probe has the highest proportion, with a value of 7.51% compared to the values of the F-CN (7.34%) and F-NO_2 (7.47%). Thus, it is clearly demonstrated that the strong attracting ability of the -NO_2 group toward hydrazine could distinctly affect the preferential combination between the ester bond and hydrazine, causing the remarkable shielding effect that inhibits the hydrazinolysis and finally leads to the poor response speed. On the contrary, the F-F probe, which has the minimum shielding effect benefitting from the weakest interaction between the benzene-F group and hydrazine, greatly promoted the stereotactic approach of hydrazine toward the ester bond and boosted the hydrazinolysis reaction.

Visual detection performance of the F-CN probe toward hydrazine

To systematically investigate the effectiveness of the modulation of the combination between the recognition site and the analyte in the pre-chemical approach, the F-CN probe with the DMSO solvent, which is a typical polar aprotic solvent good for the nucleophilic detection, was selected for the detection of hydrazine solutions with concentrations up to 200 μM (Figures 4A and S24). Upon observation of the fluorescent images of the reaction, it is obvious that the green fluorescence becomes brighter with the increase in the hydrazine concentration. The photoluminescence spectrum showed a remarkable emission enhancement of the fluorescence peak, which appeared at 526 nm after reacting with different concentrations of hydrazine (0–200 μM), and this predominantly contributes to the green fluorescence (Figure 4B). It should be noted that although the fluorescence intensity change is not remarkable when the concentration of hydrazine is 2 μM, the change in brightness in the fluorescence images taken in this low concentration range can be obviously observed (inset in Figure 4B). The fluorescence intensity rapidly increases when the hydrazine concentration is below 50 μM and tends to be saturated with the further increase in the hydrazine concentration (Figure 4C). To carefully investigate the increasing behavior of the intensity in the range of 0–10 μM, the fluorescence intensity and the hydrazine concentration was fitted linearly. This linear range was applied to the LOD (defined as LOD = $3\sigma/k$, where k is the slope of the linear part of the calibration curve [6,357], and σ is the standard deviation of noise [3]) toward

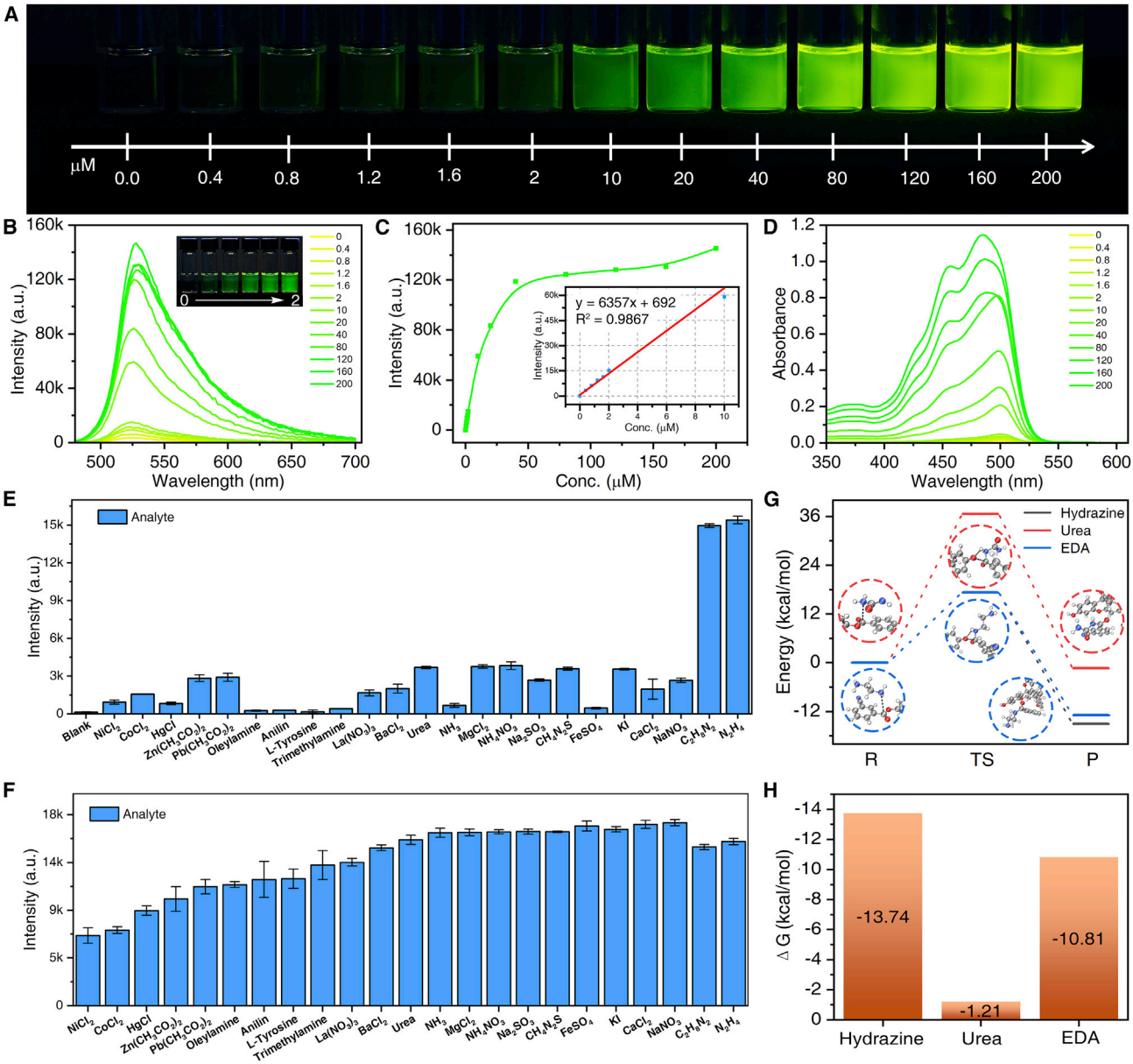

Figure 4. Fluorescent detection performance of the F-CN probe toward hydrazine

(A) Optical image of hydrazine (0–200 μM) detected by the F-CN probe under a 365-nm UV lamp irradiation.

(B) Fluorescence spectra obtained for the F-CN probe in response to different concentrations of hydrazine (0–200 μM).

(C) The fluorescence response intensities at 526 nm for the corresponding detection of different concentrations of hydrazine (0–200 μM) (inset: the linear fitting of the fluorescence response intensities toward 0–10 μM hydrazine).

(D) UV-visible (vis) absorption spectra obtained for the F-CN probe in response to different concentrations of hydrazine (0–200 μM).

(E) Fluorescence intensity changes with error bars of standard deviation from three parallel tests obtained for the F-CN probe in response to 1 mM various analytes and 2 μM hydrazine.

(F) Fluorescence intensity changes with error bars of standard deviation from three parallel tests obtained for the F-CN probe in response to mixtures of 1 mM various analytes and 2 μM hydrazine.

(G and H) Potential energy profiles (G) and Gibbs free energy (H) difference of reactions of the F-CN probe with hydrazine, urea, and EDA.

hydrazine was determined to be at least as low as 2 nM (64 ppt), which is much lower than the maximum limit of hydrazine (10 ppb) stipulated by the World Health Organization, indicating the superior performance of F-CN when compared to the other fluorescence turn-on detection methods. At the same time, the absorption peaks of

the released fluorescein located in the range of 430–530 nm and the corresponding intensity increases with the hydrazine concentration (Figure 4D). Although this green color would consume some of the fluorescence emission, the intrinsic green characteristic would not interfere with the green fluorescence signal, which is favorable for the detection of trace amounts of hydrazine.

To confirm the specificity of F-CN in the detection of hydrazine, >30 substances consisting of amine-group compounds, oxidants, reductants, metal ions, and structural analogs were selected as interferents (Figures 4E, S25, and S26). Upon the addition of the various analytes (1 mM), there was no obvious fluorescence emission except for the addition of ethanediamine (EDA) or 2 μM hydrazine due to their similar molecular structures and almost identical chemical properties (Figure S27). Meanwhile, statistical analysis of the fluorescence intensity at 526 nm showed that the F-CN probe had great anti-interference in the detection of hydrazine, with a concentration of 2 μM in the presence of 30 interferents of 500 times the hydrazine concentration (Figures 4F, S28, and S29). It should be noted that even due to the reaction of the high concentrations of $NiCl_2$ or $CoCl_2$ with the probe to form cobalt or nickel complexes, the fluorescence intensity could still remain above 50%. It is confusing that among all of these interferents, the F-CN probe presents remarkably different responses toward urea, EDA, and hydrazine even as they are similarly reducing amines. Through thermodynamic and kinetic DFT analyses, it was found that it is difficult for urea to react with the probe because of its high forward ΔE of 36.19 kcal/mol and low ΔG of −1.21 kcal/mol (Figures 4G and 4H). However, the relatively low forward ΔE of 16.73 kcal/mol and the favorable ΔG of −13.74 and −10.81 kcal/mol in the reaction between the F-CN probe and hydrazine or EDA are similar, showing an almost equivalent detection performance of the probe toward them but with a slight advantage for hydrazine over EDA. However, by accompanying other specific EDA recognition methods such as a dialdehyde reagent, EDA could easily be distinguished from the hydrazine. In addition, the F-CN probe is proved to be environmentally adaptable in a pH range of 6–10, greatly resistive to a 5,000 times higher concentration of the interferents, and highly repeatable for hydrazine detection (Figures S30–S33), demonstrating the promising potential for the practical application of the present interaction modulation-resulted fluorescent probe.

Portable detector for fast and on-site detection of hydrazine vapor

To further prove the applicability of the proposed fluorescent probe design strategy for the fast and on-site measurement of hydrazine, a highly integrated, cloud-connected, portable detector was built for the fast discrimination of the hydrazine vapor with the F-CN probe endowed sensing chip (Figure 5A). It is expected that the sensing chip filled with F-CN probe-endowed porous polymer foam would react with the hydrazine vapor inhaled by the air-harvesting module of the detector. The fluorescent response would be captured by a high-resolution camera with the help of the camera lens and the 365-nm UV light-emitting diode (LED) light excitation. Subsequently, the data of the fluorescent turn-on signal was analyzed internally and presented on the screen. It was found that the sensing chip could respond immediately to trace hydrazine vapor and deliver an alarming signal immediately after only 1-s air harvesting, which had reached the level of the fast response hydrazine electrical sensors (Figures 5B and S34). The brightness of the fluorescence-lightened area would increase and the size of the area would broaden within the next 6 s due to the further adsorption of the hydrazine vapor in the harvesting chamber and the reaction between the probe and the adsorbed hydrazine. With a further increase in the harvesting time with only 1 s, the brightness of the lightened area increased obviously, indicating the importance of air transportation to the total adsorption of hydrazine on the chip. The green emission could spread around the full square intensely with an air-harvesting time of 5 s,

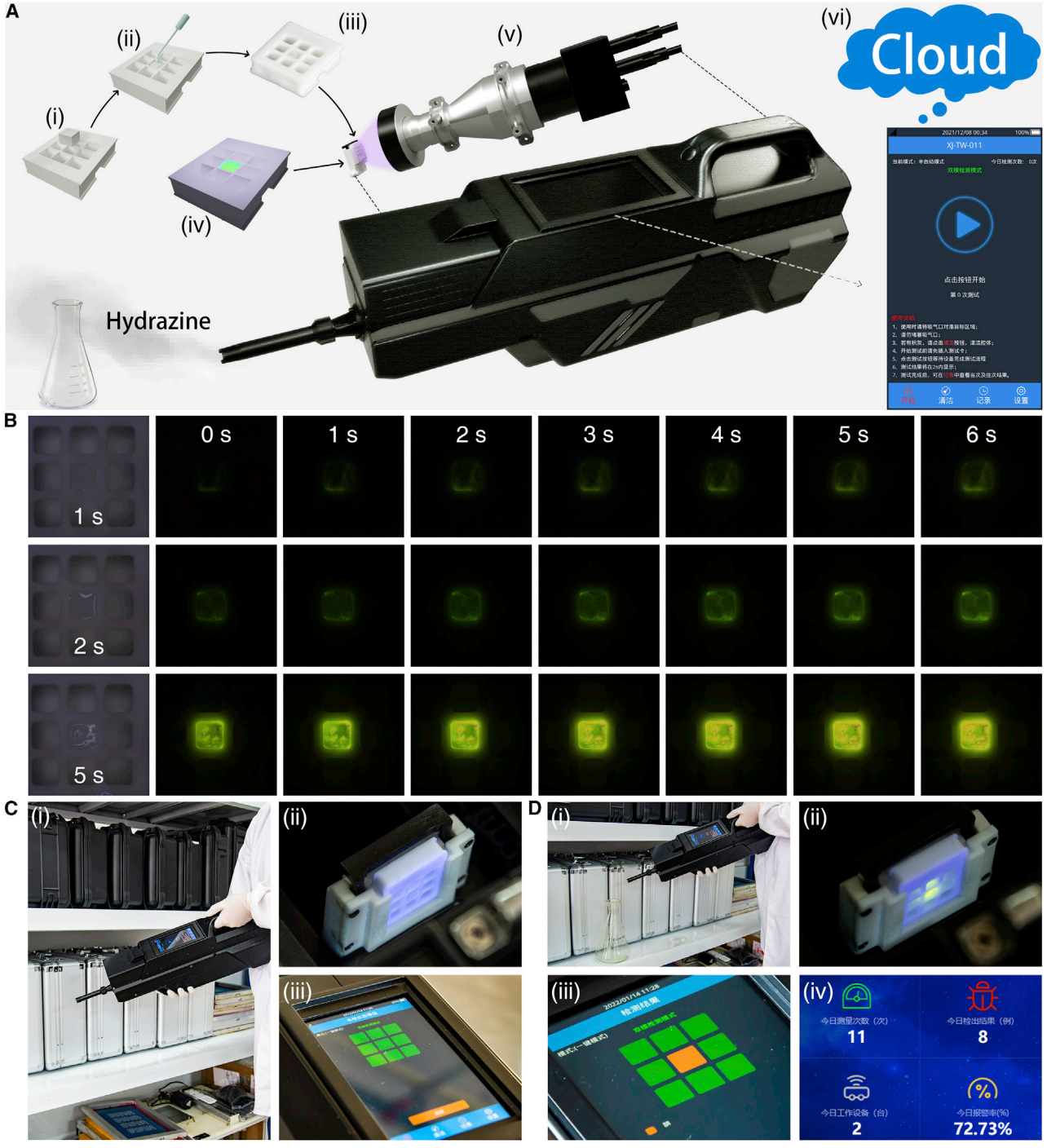

Figure 5. The F-CN probe-embedding portable detector for the fast and on-site detection of hydrazine vapor

(A) Schematic representation of the sensing chip construction and the fluorescent imaging principle of the portable detector for discrimination of the hydrazine vapor as well as the operation interface with the function of wireless data uploading.

(B) Real-time responding images of the sensing chip with 1-, 2-, and 5-s air harvesting.

(C) The simulated testing environment without hydrazine (i), the optical images of (ii) the fluorescent response of the sensing chip, and (iii) the result display on the screen of the portable detector after the test.

(D) The simulated testing environment with trace amounts of hydrazine vapor evaporated from a flat-bottomed conical laboratory flask filled with 5 mL hydrazine (i), the optical images of (ii) the green fluorescent response of the sensing chip, (iii) the hydrazine alerting display on the screen, and (iv) the uploaded data display in the cloud database.

demonstrating the great potential of the present probe design strategy for on-site hydrazine alarming. Thus, in a practical scenario, the air-harvesting time could be defined as 5 s to ensure both the reliability and the on-site detection demand. Under the circumstances, without hydrazine, the portable detector showed excellent anti-interference with no fluorescent responses on the sensing chip and no alarming (Figure 5C). While under a simulated hydrazine environment, an obvious fluorescence response could be observed on the sensing chip and a qualitative warning expressed in orange in the corresponding central square area and in the Chinese word representing hydrazine could be quickly displayed on the computer screen (Figure 5D). At the same time, the detection results were synchronously uploaded in the cloud database, in which the detection number, the positive number of the detection results, the detectors that were operating, and the alarm rate could be statistically obtained. Despite the lack of standard method, the above results clearly indicate that the designed F-CN probe is highly reliable for fast and on-site hydrazine monitoring.

DISCUSSION

In conclusion, through designing the electron-withdrawing ability of the R-benzene group adjacent to the recognition site, the interaction between the ester bond and the hydrazine was precisely modulated to promote the combination between the probe and the analyte in the pre-chemical approach process. The preferential combination of the ester bond and hydrazine was driven by the strong electrostatic combine capability and the moderate shielding effect, together with the favorable inverse Gibbs free energy barrier, ensured that the F-CN probe possessed the most effective combination and reaction with hydrazine and a boosted response speed. The modulation strategy for interaction was further seen by the specific non-fluorescent and colorless ICT probe with a LOD as low as 2 nM (64 ppt) and an ultrafast response (2–3 s light up) to hydrazine. Furthermore, the applicability of the proposed F-CN probe for the rapid, on-site, and reliable detection of hydrazine was demonstrated by the exploration of a portable fluorescence detector with promising utilization. We wish that the present interaction modulation strategy would shine a light on the exploration of high-performance fluorescent probes design for precise, ultrasensitive, and instant chemical detection.

EXPERIMENTAL PROCEDURES

Resource availability

Lead contact

Further information and requests for resources and reagents should be directed to and will be fulfilled by the lead contact, Xincun Dou (xcdou@ms.xjb.ac.cn).

Materials availability

The materials in this study will be made available upon reasonable request.

Data and code availability

The data in this study will be made available from the lead contact upon reasonable request.

Calculation and experimental method

The quantum chemical analysis in this work was performed with the Gaussian 09C,[44] Molclus code,[45] and ORCA,[46] and the wave function analyses were conducted by using Multiwfn software[47] and Shermo code.[48] The MD simulation was performed using the GROMACS package.[49] The VMD 1.9.2 program[50] was used to plot the graph. More details of the calculations and experiments are provided in the supplemental experimental procedures.

SUPPLEMENTAL INFORMATION

Supplemental information can be found online at https://doi.org/10.1016/j.xcrp.2022.100878.

ACKNOWLEDGMENTS

This work was supported by the Xinjiang Key Laboratory of Explosives Safety Science (2021D04009), the West Light Foundation of the Chinese Academy of Sciences (CAS grant no. 2020-XBQNXZ-022), the National Natural Science Foundation of China (21974150 and U1903306), the Youth Innovation Promotion Association (CAS grant no. 2018474), the Key Research Program of Frontier Sciences (CAS grant no. ZDBS-LY-JSC029), and the Natural Science Foundation of Xinjiang (2022D01E03).

AUTHOR CONTRIBUTIONS

J.L., Z.M., D.L., and X.D. conceived the research. J.L. and D.L. performed the analysis studies and device testing. The synthetic and detection experiments were performed by Z.M., with help from B.Z. D.L. and X.D. wrote the manuscript, with input from all of the other authors.

DECLARATION OF INTERESTS

The authors declare no competing interests.

Received: February 3, 2022
Revised: March 15, 2022
Accepted: April 11, 2022
Published: May 2, 2022

REFERENCES

1. Tenner, B., Zhang, J.Z., Kwon, Y., Pessino, V., Feng, S., Huang, B., Mehta, S., and Zhang, J. (2021). Fluosteps: fluorescent biosensors for monitoring compartmentalized signaling within endogenous microdomains. Sci. Adv. *7*, eabe4091. https://doi.org/10.1126/sciadv.abe4091.

2. Chatterjee, S., Ahire, K., and Karuso, P. (2020). Room-temperature dual fluorescence of a locked green fluorescent protein chromophore analogue. J. Am. Chem. Soc. *142*, 738–749. https://doi.org/10.1021/jacs.9b05096.

3. Vallan, L., Urriolabeitia, E.P., Ruiperez, F., Matxain, J.M., Canton-Vitoria, R., Tagmatarchis, N., Benito, A.M., and Maser, W.K. (2018). Supramolecular-enhanced charge transfer within entangled polyamide chains as the origin of the universal blue fluorescence of polymer carbon dots. J. Am. Chem. Soc. *140*, 12862–12869. https://doi.org/10.1021/jacs.8b06051.

4. Zhao, M., Wang, J., Lei, Z., Lu, L., Wang, S., Zhang, H., Li, B., and Zhang, F. (2021). NIR-II pH sensor with a FRET adjustable transition point for in situ dynamic tumor microenvironment visualization. Angew. Chem. Int. Ed. *60*, 5091–5095. https://doi.org/10.1002/anie.202012021.

5. Trigo-Mourino, P., Thestrup, T., Griesbeck, O., Griesinger, C., and Becker, S. (2019). Dynamic tuning of FRET in a green fluorescent protein biosensor. Sci. Adv. *5*, aaw4988. https://doi.org/10.1126/sciadv.aaw4988.

6. Patra, L., Aich, K., Gharami, S., and Mondal, T.K. (2021). Fabrication of a new fluorogenic probe for detection of phosgene in solution and vapor phase. Sens. Actuators B Chem. *326*, 128837. https://doi.org/10.1016/j.snb.2020.128837.

7. Ma, Z., Li, J., Hu, X., Cai, Z., and Dou, X. (2020). Nitrite detection: ultrasensitive, specific, and rapid fluorescence turn-on nitrite sensor enabled by precisely modulated fluorophore binding. Adv. Sci. *7*, 2070133. https://doi.org/10.1002/advs.202070133.

8. Su, Z., Li, Y., Li, J., and Dou, X. (2021). Ultrasensitive luminescent turn-on detection of perchlorate particulates by triggering supramolecular self-assembly of platinum(II) complex in hydrogel matrix. Sens. Actuators B Chem. *336*, 129728. https://doi.org/10.1016/j.snb.2021.129728.

9. Persch, E., Dumele, O., and Diederich, F. (2015). Molecular recognition in chemical and biological systems. Angew. Chem. Int. Ed. *54*, 3290–3327. https://doi.org/10.1002/anie.201408487.

10. Kengmana, E.S., Lee, J.K., Li, X., Warner, J.H., and Han, G.G.D. (2020). Self-assembly of bowlic supramolecules on graphene imaged at the individual molecular level using heavy atom tagging. Small *16*, 2002860. https://doi.org/10.1002/smll.202002860.

11. Lei, Y., Zhang, G., Zhang, Q., Yu, L., Li, H., Yu, H., and He, Y. (2021). Visualization of gaseous iodine adsorption on single zeolitic imidazolate framework-90 particles. Nat. Commun. *12*, 4483. https://doi.org/10.1038/s41467-021-24830-1.

12. Blanco, E., Martínez, J.I., Parra-Alfambra, A.M., Petit-Domínguez, M.D., del Pozo, M., Martín-Gago, J.A., Casero, E., and Quintana, C. (2019). Fluorescence enhancement of fungicide thiabendazole by van der Waals interaction with transition metal dichalcogenide nanosheets for highly specific sensors. Nanoscale *11*, 23156–23164. https://doi.org/10.1039/c9nr02794g.

13. Satake, A. (2020). The solvent effect on weak interactions in supramolecular polymers: Differences between small molecular probes and supramolecular polymers. ChemPlusChem *85*, 1542–1548. https://doi.org/10.1002/cplu.202000400.

14. Dong, Q., Qu, W., Wang, P., and Wong, W.-Y. (2016). A novel supramolecular system with multiple fluorescent states constructed by orthogonal self-assembly. Polym. Chem. *7*, 3827–3831. https://doi.org/10.1039/c6py00542j.

15. Qayyum, M., Bushra, T., Khan, Z.A., Gul, H., Majeed, S., Yu, C., Farooq, U., Shaikh, A.J., and Shahzad, S.A. (2021). Synthesis and tetraphenylethylene-based aggregation-induced emission probe for rapid detection of nitroaromatic compounds in aqueous media. ACS Omega *6*, 25447–25460. https://doi.org/10.1021/acsomega.1c03439.

16. Silvi, S., and Credi, A. (2015). Luminescent sensors based on quantum dot–molecule

conjugates. Chem. Soc. Rev. *44*, 4275–4289. https://doi.org/10.1039/c4cs00400k.

17. Wang, H., Ji, X., Li, Z., and Huang, F. (2017). Fluorescent supramolecular polymeric materials. Adv. Mater. *29*, 1606117. https://doi.org/10.1002/adma.201606117.

18. Ma, Z., Li, J., Hu, X., Cai, Z., and Dou, X. (2020). Ultrasensitive, specific, and rapid fluorescence turn-on nitrite sensor enabled by precisely modulated fluorophore binding. Adv. Sci. *7*, 2002991. https://doi.org/10.1002/advs.202002991.

19. Liu, K., Shang, C., Wang, Z., Qi, Y., Miao, R., Liu, K., Liu, T., and Fang, Y. (2018). Non-contact identification and differentiation of illicit drugs using fluorescent films. Nat. Commun. *9*, 1695. https://doi.org/10.1038/s41467-018-04119-6.

20. Chi, W., Chen, J., Liu, W., Wang, C., Qi, Q., Qiao, Q., Tan, T.M., Xiong, K., Liu, X., Kang, K., et al. (2020). A general descriptor ΔE enables the quantitative development of luminescent materials based on photoinduced electron transfer. J. Am. Chem. Soc. *142*, 6777–6785. https://doi.org/10.1021/jacs.0c01473.

21. Wan, H., Xu, Q., Gu, P., Li, H., Chen, D., Li, N., He, J., and Lu, J. (2021). AIE-based fluorescent sensors for low concentration toxic ion detection in water. J. Hazard. Mater. *403*, 123656. https://doi.org/10.1016/j.jhazmat.2020.123656.

22. Fan, S., Zhang, G., Dennison, G.H., FitzGerald, N., Burn, P.L., Gentle, I.R., and Shaw, P.E. (2020). Challenges in fluorescence detection of chemical warfare agent vapors using solid-state films. Adv. Mater. *32*, 1905785. https://doi.org/10.1002/adma.201905785.

23. Xu, W., Li, X., Yin, J., Liu, W., Yang, Y., and Li, W. (2019). A new fluorescent turn-on dual interaction position probe for determination of hydrazine. Anal. Sci. *35*, 1341–1345. https://doi.org/10.2116/analsci.19p229.

24. Vijay, N., and Velmathi, S. (2020). Near-infrared-emitting probes for detection of nanomolar hydrazine in a complete aqueous medium with real-time application in bioimaging and vapor-phase hydrazine detection. ACS Sustain. Chem. Eng. *8*, 4457–4463. https://doi.org/10.1021/acssuschemeng.9b07445.

25. Qu, D.Y., Chen, J.L., and Di, B. (2014). A fluorescence "switch-on" approach to detect hydrazine in aqueous solution at neutral ph. Anal. Methods *6*, 4705–4709. https://doi.org/10.1039/c4ay00533c.

26. Lu, Z., Fan, W., Shi, X., Lu, Y., and Fan, C. (2017). Two distinctly separated emission colorimetric nir fluorescent probe for fast hydrazine detection in living cells and mice upon independent excitations. Anal. Chem. *89*, 9918–9925. https://doi.org/10.1021/acs.analchem.7b02149.

27. Lee, M.H., Yoon, B., Kim, J.S., and Sessler, J.L. (2013). Naphthalimide trifluoroacetyl acetonate: a hydrazine-selective chemodosimetric sensor. Chem. Sci. *4*, 4121–4126. https://doi.org/10.1039/c3sc51813b.

28. Cui, L., Peng, Z., Ji, C., Huang, J., Huang, D., Ma, J., Zhang, S., Qian, X., and Xu, Y. (2014). Hydrazine detection in the gas state and aqueous solution based on the gabriel mechanism and its imaging in living cells. Chem. Commun. *50*, 1485–1487. https://doi.org/10.1039/c3cc48304e.

29. Liu, Y., Perez, L., Mettry, M., Gill, A.D., Byers, S.R., Easley, C.J., Bardeen, C.J., Zhong, W., and Hooley, R.J. (2017). Site selective reading of epigenetic markers by a dual-mode synthetic receptor array. Chem. Sci. *8*, 3960–3970. https://doi.org/10.1039/c7sc00865a.

30. Sarfo, D.K., Izake, E.L., O'Mullane, A.P., and Ayoko, G.A. (2018). Molecular recognition and detection of Pb(II) ions in water by amino-benzo-18-crown-6 immobilised onto a nano-structured sers substrate. Sens. Actuators B Chem. *255*, 1945–1952. https://doi.org/10.1016/j.snb.2017.08.223.

31. Cheng, C., Gong, Y., Guo, Y., Cui, L., Ji, H., Yuan, H., Jiang, L., Zhao, J., and Che, Y. (2021). Long-range exciton migration in coassemblies: achieving high photostability without disrupting the electron donation of fluorene oligomers. Angew. Chem. Int. Ed. *60*, 5827–5832. https://doi.org/10.1002/anie.202012474.

32. Chen, Z., Tian, Z., Kallio, K., Oleson, A.L., Ji, A., Borchardt, D., Jiang, D.E., Remington, S.J., and Ai, H.W. (2016). The N–B interaction through a water bridge: understanding the chemoselectivity of a fluorescent protein based probe for peroxynitrite. J. Am. Chem. Soc. *138*, 4900–4907. https://doi.org/10.1021/jacs.6b01285.

33. Yue, Y., Huo, F., Ning, P., Zhang, Y., Chao, J., Meng, X., and Yin, C. (2017). Dual-site fluorescent probe for visualizing the metabolism of cys in living cells. J. Am. Chem. Soc. *139*, 3181–3185. https://doi.org/10.1021/jacs.6b12845.

34. Chen, L., Tian, X., Zhao, Y., Li, Y., Yang, C., Zhou, Z., and Liu, X. (2016). A ratiometric fluorescence nanosensor for highly selective and sensitive detection of selenite. Analyst *141*, 4685–4693. https://doi.org/10.1039/c6an00740f.

35. Zhu, S., Li, X., Jiao, X., Shao, W., Li, L., Zu, X., Hu, J., Zhu, J., Yan, W., Wang, C., et al. (2021). Selective CO_2 photoreduction into C2 product enabled by charge-polarized metal pair sites. Nano Lett. *21*, 2324–2331. https://doi.org/10.1021/acs.nanolett.1c00383.

36. Li, H., Miao, X., Zhang, J., Du, J., Xu, S., Tang, J., and Zhang, Y. (2020). Dft studies on the reaction mechanism and kinetics of dibutyl phthalate initiated by hydroxyl and sulfate radicals: prediction of the most reactive sites. Chem. Eng. J. *381*, 122680. https://doi.org/10.1016/j.cej.2019.122680.

37. Fu, W., Wang, Q., Chen, W., Qian, G., Zhang, J., Chen, D., Yuan, W., Zhou, X., and Duan, X. (2021). Engineering Ru atomic structures toward enhanced kinetics of hydrogen generation. Chem. Eng. Sci. *235*, 116507. https://doi.org/10.1016/j.ces.2021.116507.

38. Qi, J., Chen, C., Zhang, X., Hu, X., Ji, S., Kwok, R.T.K., Lam, J.W.Y., Ding, D., and Tang, B.Z. (2018). Light-driven transformable optical agent with adaptive functions for boosting cancer surgery outcomes. Nat. Commun. *9*, 1848. https://doi.org/10.1038/s41467-018-04222-8.

39. Roy, B., and Bandyopadhyay, S. (2018). The design strategies and mechanisms of fluorogenic and chromogenic probes for the detection of hydrazine. Anal. Methods *10*, 1117–1139. https://doi.org/10.1039/c7ay02866k.

40. Teng, M., Zhou, Z., Qin, Y., Zhao, Y., Zhao, C., and Cao, J. (2020). A water-soluble fluorescence sensor with high specificity for detecting hydrazine in river water detection and a549 cell imaging. Sens. Actuators B Chem. *311*, 127914. https://doi.org/10.1016/j.snb.2020.127914.

41. Li, Z., Zhang, W., Liu, C., Yu, M., Zhang, H., Guo, L., and Wei, L. (2017). A colorimetric and ratiometric fluorescent probe for hydrazine and its application in living cells with low dark toxicity. Sens. Actuators B Chem. *241*, 665–671. https://doi.org/10.1016/j.snb.2016.10.141.

42. Zhang, F., Li, D., Liang, X., Guo, K., Li, B., Xu, H., Li, J., Zhang, Z., Wang, S., Fan, F., and Sun, Y. (2021). Forming luminescent oligomer nanoparticles via condensation polymerization: a strategy for real-time visualized detection of hydrazine in solution and gas phase. Dyes Pigm. *185*, 108931. https://doi.org/10.1016/j.dyepig.2020.108931.

43. Li, J., Cui, Y., Bi, C., Feng, S., Yu, F., Yuan, E., Xu, S., Hu, Z., Sun, Q., Wei, D., and Yoon, J. (2019). Oligo(ethylene glycol)-functionalized ratiometric fluorescent probe for the detection of hydrazine in vitro and in vivo. Anal. Chem. *91*, 7360–7365. https://doi.org/10.1021/acs.analchem.9b01223.

44. Frisch, M.J., Trucks, G.W., Schlegel, H.B., Scuseria, G.E., Robb, M.A., Cheeseman, J.R., Scalmani, G., Barone, V., Petersson, G.A., Nakatsuji, H., et al. (2016). Gaussian 09, Revision C.01.

45. Lu, T. (2021). Molclus Program, Version 1.9.9.7. http://www.keinsci.com/research/molclus.html.

46. Neese, F. (2018). Software update: the ORCA program system, version 4.0. Wires Comput. Mol. Sci. *8*, e1327. https://doi.org/10.1002/wcms.1327.

47. Lu, T., and Chen, F.W. (2012). Multiwfn: a multifunctional wavefunction analyzer. J. Comput. Chem. *33*, 580–592. https://doi.org/10.1002/jcc.22885.

48. Lu, T., and Chen, Q. (2021). Shermo: a general code for calculating molecular thermochemistry properties. Comput. Theor. Chem. *1200*, 113249. https://doi.org/10.1016/j.comptc.2021.113249.

49. Berendsen, H.J.C., van der Spoel, D., and van Drunen, R. (1995). Gromacs: a message-passing parallel molecular dynamics implementation. Comput. Phys. Commun. *91*, 43–56. https://doi.org/10.1016/0010-4655(95)00042-e.

50. Humphrey, W., Dalke, A., and Schulten, K. (1996). VMD: visual molecular dynamics. J. Mol. Graph. Model. *14*, 33–38. https://doi.org/10.1016/0263-7855(96)00018-5.